Supporting Information

Choi et al. 10.1073/pnas.1103573108

SI Text

Surface Charge of Unmodified Gold Nanoparticles. For any charged sphere of radius R in an electrolyte, its ζ-potential is given as follows (Eq. S1):

$$\zeta = \frac{\sigma}{\varepsilon}\frac{R}{1+\kappa R}. \quad [S1]$$

Above, σ, ε, and κ^{-1} are the surface charge density, permittivity constant, and Debye length.

From this equation, ζ of charged gold spheres becomes more negative as R increases, consistent with data shown in Table 1. For typical ζ measurements in 1 mM KCl at room temperature, κ^{-1} is roughly 9.8 nm, a constant independent of R. By curve fitting of the measured ζ as a function of R, the dimensionless charge density (σ/ε) is ∼3. This means that unmodified gold surface of all sizes has a constant surface charge density.

PEG Corona Thickness of PEGylated Gold Nanoparticles. Based on a previous work by Takae et al. (1), each 20-nm gold-based nanoparticle (AuNP) can anchor 520 PEG chains of 6,000 Da each. This translates to a PEG grafting density (Σ) of 0.4 PEG/nm^2.

The Kuhn length (b) of PEG is 0.7 nm. Thus, the dimensionless PEG grafting density (σ*) is as follows (Eq. S2):

$$\sigma^* = b^2\Sigma = (0.7\text{nm})^2\left(0.4\ \text{PEG/nm}^2\right) = 0.196. \quad [S2]$$

Hill et al. (2) evaluated the grafting density of oligonucleotides on submicron-sized AuNPs (10–100 nm). If the oligonucleotide density data because of size curvature is applicable to the study of PEG grafting, then a rough estimate of PEG grafting density of Au_x-PEG_y NPs is provided in Table S1.

σ* takes on the value of 0.1–0.2 (for AuNPs above the size of 20 nm), which represents a very high grafting density according to Wijmans and Zhulina (3). Physically, how high is this density? According to scaling analysis by deGennes (4) on grafted polymers, the brush conformation appears if $\sigma^* > N^{-6/5}$, where N is the number of Kuhn polymer segments. How can we estimate N? Take Au_{50}-$PEG_{5,000}$ NPs as an example. The molecular weight of each PEG unit is 44 g/mol. The two C-O bonds (each 0.145 nm) and the C-C bond (0.15 nm) add up to 0.44 nm. The contour length ($R_{max} = Nb$) of a fully stretched $PEG_{5,000}$ coil is 5,000/44 × 0.44 nm = 50 nm. If b = 0.7 nm (two times the persistent length of PEG) (5), then n = 71.4. Clearly, σ* is greater than $N^{-6/5}$. Hence, PEG polymer chains are overlapping with each other, with their blobs acting as hard spheres that cover the gold surface densely. The $\sigma^* > N^{-6/5}$ result is also apparent for all other Au_x-PEG_y NPs. Alternatively, one can calculate the footprint (D) of each PEG chain (separation distance between each adjacent PEG chain) on the gold surface knowing that $4\pi D^2 = \Sigma$. For Au_{50}-$PEG_{5,000}$ NPs, D = 2.29 nm, which is shorter than the Flory radius of $PEG_{5,000}$ in a good solvent ($R_F = bN^{3/5}$ = 9.07 nm). Because the $R_F > D$ result is apparent for all other Au_x-PEG_y NPs, the grafted PEG chains all take the brush conformation on the gold surface for all particle sizes.

On a planar surface, the brush height of tethered PEG corona (H) should scale linearly with N (4, 6). However, on a spherical interface, $H \sim N^{3/5}$, because the chains extended away from the surface should be more diffuse compared with those densely packed chains near the surface, thus shortening H. However, DLS measurements revealed that $H \sim N$ and not $H \sim N^{3/5}$, suggesting that the curvature effect on H is not eminent. For σ* ∼ 0.1 and using self-consistence field simulations, Dan and Tirrell (7) showed that the curvature effect becomes less important and that H will approach the planar limit of $H \sim N$ when $x/2b >$ 100. For Au_x-PEG_y NPs at hand, their values of $x/2b$ mainly lie in the range of 28–57, and therefore, $H \sim N^{0.9}$ according to simulation results by Dan and Tirrell (7). This explains the observed approximate linearity between H and N, even on spherical particles.

1. Takae S, et al. (2005) Ligand density effect on biorecognition by PEGylated gold nanoparticles: Regulated interaction of RCA120 lectin with lactose installed to the distal end of tethered PEG strands on gold surface. *Biomacromolecules* 6:818–824.
2. Hill HD, Millstone JE, Banholzer MJ, Mirkin CA (2009) The role radius of curvature plays in thiolated oligonucleotide loading on gold nanoparticles. *ACS Nano* 3:418–424.
3. Wijmans CM, Zhulina EB (1993) Polymer brushes at curved interfaces. *Macromolecules* 26:7214–7224.
4. deGennes PG (1980) Conformations of polymers attached to an interface. *Macromolecules* 13:1069–1075.
5. Kienberger F, et al. (2000) Static and dynamical properties of single poly(ethylene glycol) molecules investigated by force microscopy. *Single Mol* 1:123–128.
6. Alexander SA (1977) Adsorption of chain molecules with a polar head: A scaling description. *J Phys France* 38:983–987.
7. Dan N, Tirrell M (1992) Polymers tethered to curved interfaces. A self-consistent-field analysis. *Macromolecules* 25:2890–2895.

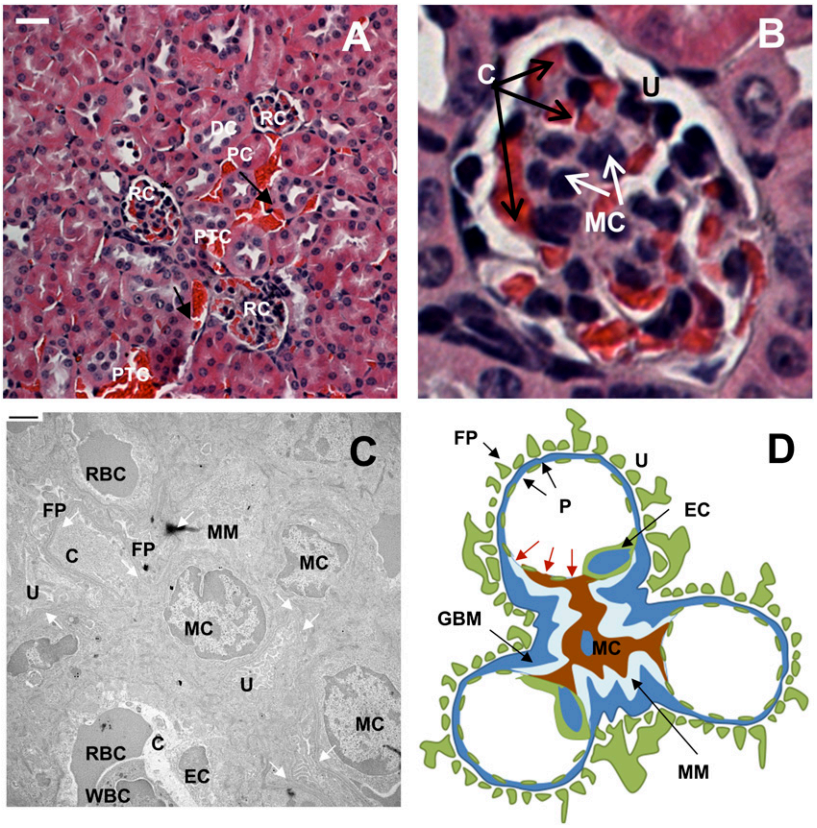

Fig. S1. Structure of the renal corpuscle and mesangium. Illustrations of the renal corpuscle and the mesangium. (*A*) This light micrograph reveals the typical morphology of the renal cortex. (Scale bar: 10 μm.) (*B*) This close-up figure reveals the inner structure of a renal corpuscle. (*C*) This transmission electron micrograph shows the internal structures of the renal corpuscles. (Scale bar: 10 μm.) (*D*) This schematic diagram shows the relationship between mesangial cells and glomerular capillaries (modified from ref. 1). C, glomerular capillary space; DC, distal convoluted tubules; EC, endothelial cell; FP, foot processes of podocytes; GBM, glomerular basement membrane; MC, mesangial cells; MM, mesangial matrix; P, pores of the fenestrated endothelium of glomerular capillaries; PC, proximal convoluted tubules; PTC, peritubular capillaries; RBC, red blood cells; RC, renal corpuscles; WBC, leukocytes; U, urinary space. In *C*, white arrows trace the glomerular basement membrane. In *D*, red arrows indicate the pores between the glomerular capillaries and mesangium. If smaller than the pore width, particles can enter the mesangium from the glomerular capillaries in the absence of GBM and podocytes as structural barriers.

1. Sakai T, Kriz W (1987) The structural relationship between mesangial cells and basement membrane of the renal glomerulus. *Anat Embryol (Berl)* 176:373–386.

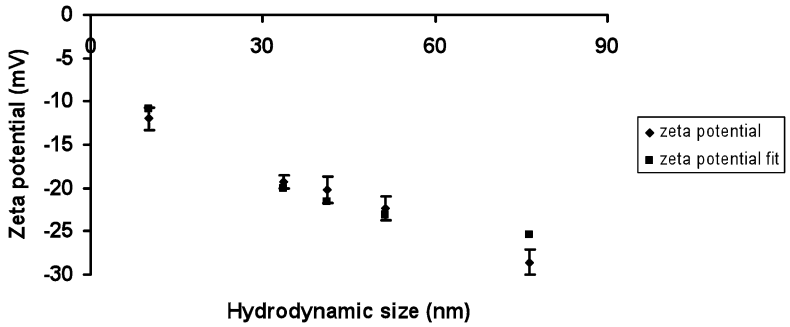

Fig. S2. Dynamic light scattering (DLS) measurements of ζ of unmodified gold nanoparticle match reasonably with estimates based on Debye–Huckel electrokinetic theory.

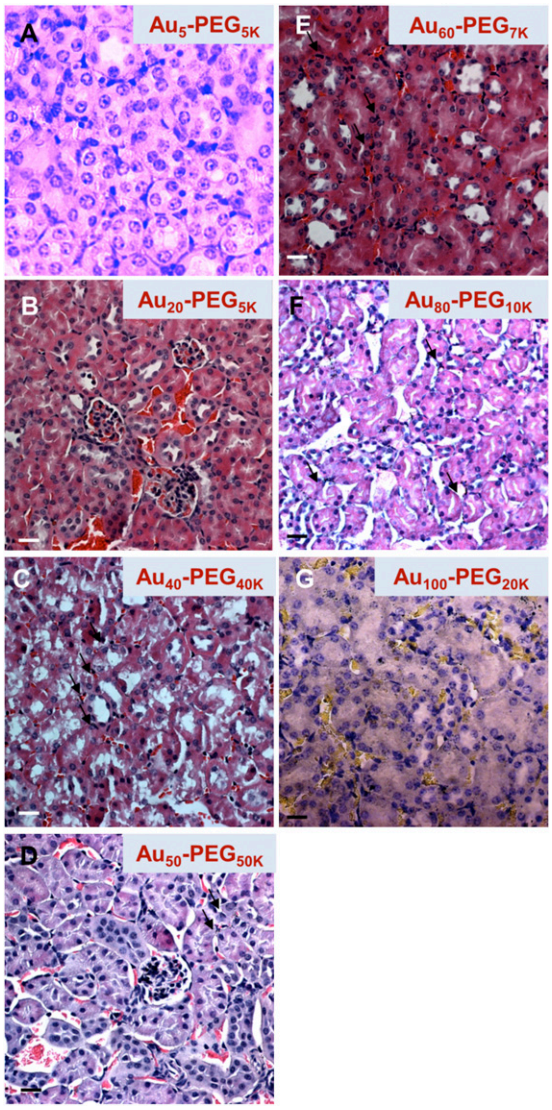

Fig. S3. Tissue-level accumulation of PEG-AuNPs of different sizes (*A*–*G*) in peritubular capillaries. The deposition of PEGylated gold nanoparticles in the renal cortex excluding renal corpuscles is not a function of particle size. Typically, particles are located adjacent to peritubular capillaries or in the connective tissue space between adjacent convoluted tubule cells. (Scale bar: 10 μm.)

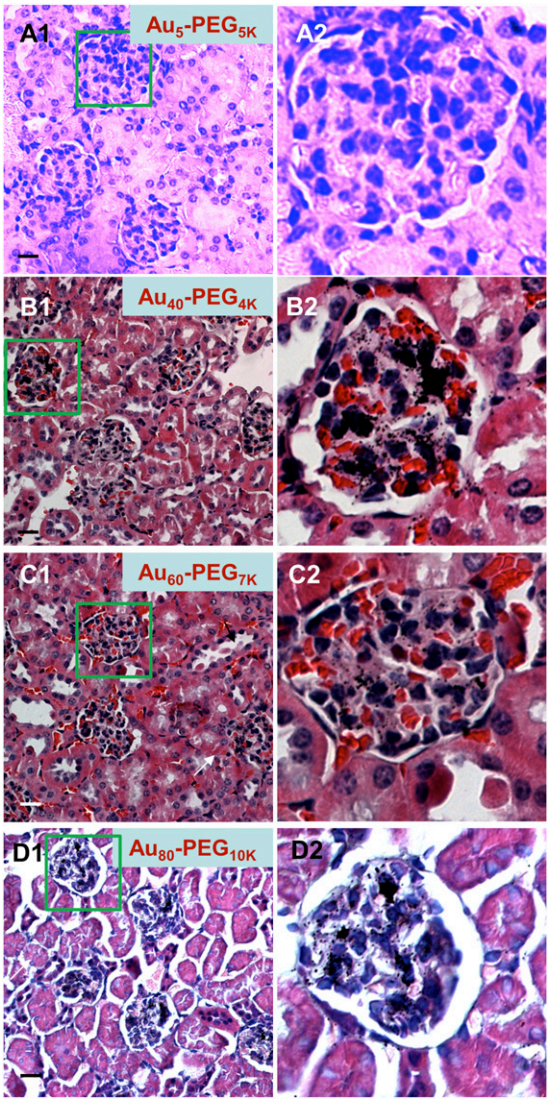

Fig. S4. Tissue-level accumulation of PEG-AuNPs in renal corpuscles. The deposition of PEGylated gold nanoparticles in renal corpuscles is a strong function of particle size. *Right* illustrates the magnified renal corpuscle (green box) shown in *Left*. (*A*) The smallest particles (Au_5-PEG_{5K}) showed undetectable staining. (*B* and *C*) Middle-sized particles (Au_{40}-PEG_{4K} and Au_{60}-PEG_{7K}) showed the most intense silver staining near the mesangial cells throughout the entire renal corpuscle. (*D*) Larger particles (Au_{80}-PEG_{10K}) showed intense staining but at a reduced areal fraction of the renal corpuscles. (Scale bar: 10 μm.)

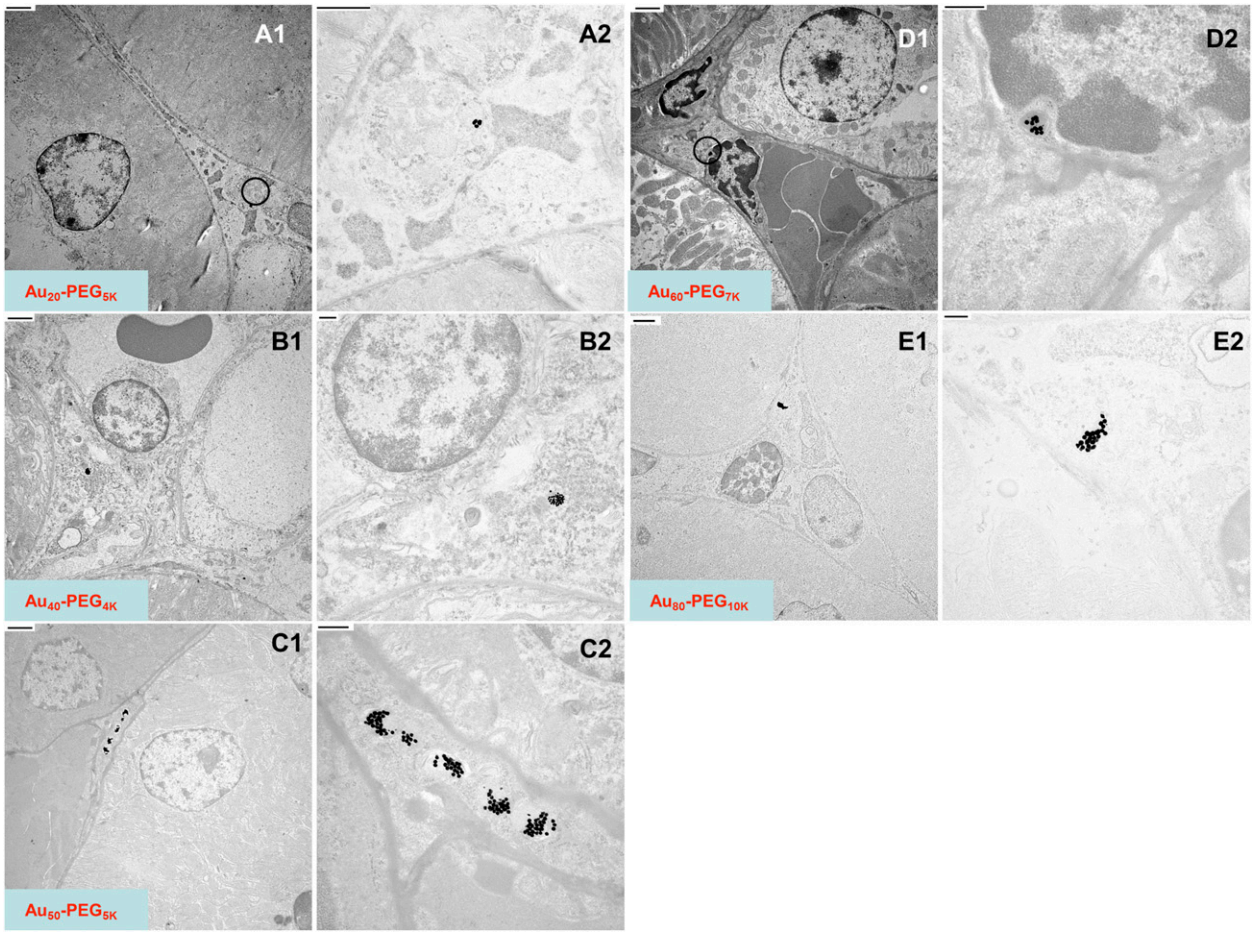

Fig. S5. Cellular-level accumulation of PEG-AuNPs of different sizes (*A–E*) in peritubular capillaries. The deposition of Au_x-PEG_y NPs in the renal cortex excluding renal corpuscles is not a function of particle size. Particles are located adjacent to peritubular capillaries or in the connective tissue space between convoluted tubule cells. Images shown in *Right* are magnified versions of those shown in *Left*. (Scale bar: *Left*, 2 μm; *Right*, 500 nm.)

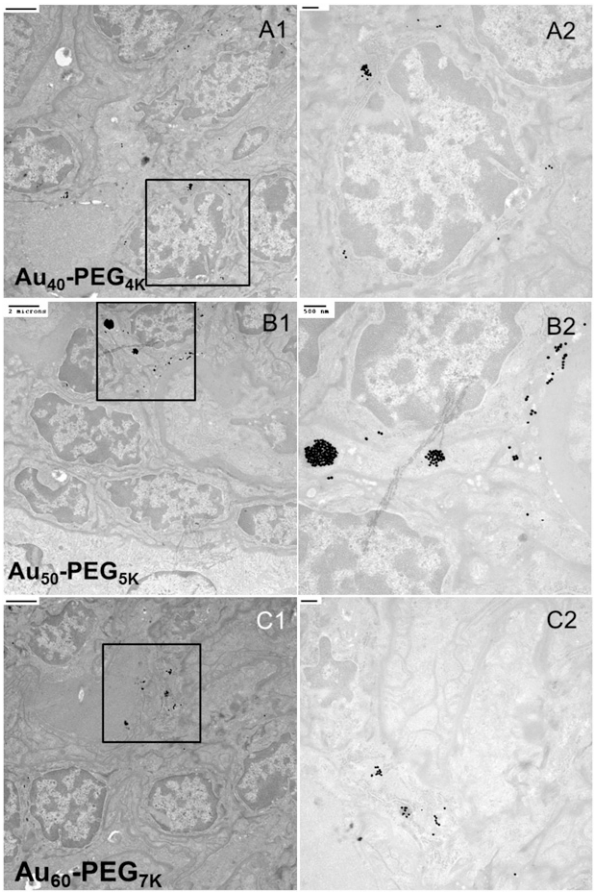

Fig. S6. Cellular-level accumulation of PEG-AuNPs in renal corpuscles. The deposition of Au_x-PEG_y NPs in the renal corpuscles is size-dependent. Middle-sized particles [(*A*) Au_{40}-PEG_{4K}, (*B*) Au_{50}-PEG_{5K}, and (*C*) Au_{60}-PEG_{7K} NPs] accumulated within mesangial cells or in the mesangium as individual entities at the maximal amount. Images shown in *Right* show the magnified portions (black box) in *Left*. (Scale bar: *Left*, 2 μm; *Right*, 500 nm.)

Table S1. Rough estimates of PEG grafting density on Au_x-PEG_y NPs of different sizes

x (nm)	β (no. of oligo/nm^2)	Σ (no. of PEG/nm^2)	σ^*
20	1.4×10^{13}	0.400	0.196
40	8.5×10^{12}	0.243	0.119
50	8.1×10^{12}	0.231	0.113
60	7.8×10^{12}	0.223	0.109
80	7.1×10^{12}	0.203	0.099

x, core size of gold nanoparticles; β, oligonucleotide grafting density [all entries referenced from Hill et al. (2)]; Σ, PEG grafting density [with the first entry (0.4) by Takae et al. (1) and all remaining entries scaled according to β]; $\sigma^* = b^2\Sigma$ [dimensionless PEG grafting density (with the first entry of 0.196 determined on Page 1 and all remaining entries scaled according to Σ)].

Table S2. Polymer parameters of grafted PEG on AuNPs

	Au_{40}-PEG_{4K}	Au_{50}-PEG_{5K}	Au_{60}-PEG_{7K}	Au_{80}-PEG_{10K}
MW (g/mol)	4,000	5,000	7,000	10,000
R_{max} (nm)	40	50	70	100
N	57.14	71.43	100	142.86
$N^{-6/5}$	0.0078	0.0060	0.0040	0.0026
R_F (nm)	7.93	9.07	11.09	13.74
D (nm)	2.29	2.35	2.39	2.50
x (nm)	40	50	60	80
$x/2b$	28.57	35.71	42.86	57.14

D, separation distance between adjacent PEG monomers; MW, molecular weight of grafted PEG; N, degree of polymerization (number of Kuhn segments); $R_F = bN^{3/5}$ (Flory radius in a good solvent); $R_{max} = bN$ (contour length); x, core size of AuNP.

Table S3. Blood pharmacokinetics of Au_x-PEG_y NPs

t (h)	Au_5-PEG_{5K}	Au_{20}-PEG_{5K}	Au_{40}-PEG_{4K}	Au_{50}-PEG_{5K}	Au_{60}-PEG_{7K}	Au_{80}-PEG_{10K}	Au_{100}-PEG_{20K}
0.5	57.36 ± 4.53	64.84 ± 11.30	78.04 ± 7.04	91.61 ± 7.53	83.83 ± 13.96	73.96 ± 9.85	49.04 ± 7.31
4	47.83 ± 3.74	46.97 ± 9.67	66.14 ± 5.89	81.31 ± 4.98	71.42 ± 8.46	64.12 ± 6.39	35.44 ± 3.27
24	40.83 ± 6.60	38.43 ± 9.91	23.45 ± 7.73	27.22 ± 5.71	19.54 ± 3.94	10.97 ± 3.80	7.48 ± 1.26

Mean gold contents and SDs are normalized to percent injected dose (% ID) measured from three mice for each Au_x-PEG_y NP class.

Table S4. Organ-level distribution of Au_x-PEG_y NPs 24 h after dosing

Organ	Au_5-PEG_{5K}	Au_{20}-PEG_{5K}	Au_{40}-PEG_{4K}	Au_{50}-PEG_{5K}	Au_{60}-PEG_{7K}	Au_{80}-PEG_{10K}	Au_{100}-PEG_{20K}
Kidney	0.19 ± 0.05	1.16 ± 0.48	3.01 ± 0.64	4.62 ± 0.98	1.92 ± 0.43	0.74 ± 0.37	0.55 ± 0.25
Spleen	2.55 ± 0.56	4.86 ± 2.21	13.23 ± 3.89	8.94 ± 2.31	11.82 ± 4.31	16.42 ± 5.42	20.41 ± 4.31
Lung	3.06 ± 0.77	0.36 ± 0.14	0.36 ± 0.23	1.31 ± 0.72	0.16 ± 0.06	0.68 ± 0.14	0.19 ± 0.03
Heart	0.36 ± 0.18	0.31 ± 0.23	0.26 ± 0.10	0.91 ± 0.42	0.07 ± 0.01	0.21 ± 0.02	0.07 ± 0.01
Liver	14.71 ± 3.36	20.64 ± 6.66	38.86 ± 5.06	31.99 ± 5.48	37.31 ± 5.23	48.02 ± 7.73	61.94 ± 7.81
Pancreas	2.52 ± 0.64	0.23 ± 0.07	0.15 ± 0.04	1.29 ± 0.38	0.05 ± 0.02	0.26 ± 0.02	0.06 ± 0.03
Blood	40.83 ± 6.60	38.43 ± 9.91	23.45 ± 7.73	27.22 ± 5.71	19.54 ± 3.94	10.97 ± 3.80	7.48 ± 1.26

Mean gold contents and SDs are normalized to percent injected dose (% ID) measured from three mice for each Au_x-PEG_y NP class.